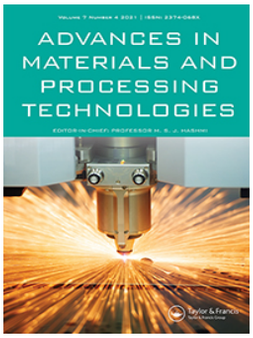

Taylor & Francis
Taylor & Francis Group

Advances in Materials and Processing Technologies

ISSN: (Print) (Online) Journal homepage: https://www.tandfonline.com/loi/tmpt20

Investigation of electrochemical discharge machining process variables during μ - drilling on stir casted novel Zn/ (Ag+ Fe)-MMC for biomedical applications

Inderjeet Singh Sandhu, Saurabh Kumar Maurya & Alakesh Manna

To cite this article: Inderjeet Singh Sandhu, Saurabh Kumar Maurya & Alakesh Manna (2022): Investigation of electrochemical discharge machining process variables during μ - drilling on stir casted novel Zn/ (Ag+ Fe)-MMC for biomedical applications, Advances in Materials and Processing Technologies, DOI: 10.1080/2374068X.2022.2139895

To link to this article: https://doi.org/10.1080/2374068X.2022.2139895

Published online: 29 Oct 2022.

ADVANCES IN MATERIALS AND PROCESSING TECHNOLOGIES
https://doi.org/10.1080/2374068X.2022.2139895

Investigation of electrochemical discharge machining process variables during μ - drilling on stir casted novel Zn/ (Ag+ Fe)-MMC for biomedical applications

Inderjeet Singh Sandhu, Saurabh Kumar Maurya and Alakesh Manna

Department of Mechanical Engineering, Punjab Engineering College (Deemed to be University), Chandigarh, India

ABSTRACT

Stainless steel, titanium alloy, and cobalt have long-term risks when used as metallic implants. Zinc is essential component of human body and can be used for metallic implants. The research presents the fabrication of novel hybrid Zn/(Ag + Fe)-MMC using stir casting method, analysis of microstructural and mechanical properties of fabricated MMC specimen. Electrochemical Discharge Machining (ECDM) was employed for the μ-drilling on the fabricated MMC. The effect of ECDM process variables like supply voltage, peak current, pulse-on-time, pulse-off-time, feed rate and electrolyte concentration on material removal rate (MRR), overcut (OC) and tool wear (TW) were identified during μ-drilling. Experiments had been performed based on the one factor-at-a-time approach. From the experiments it was found that MRR, OC and TW increase as supply voltage, peak current, pulse-on-time, electrolyte concentration increase and decrease as pulse-off-time increases. An increment in feed rate increases the MRR and TW but overcut decreases. Scanning electron microscopy (SEM) analysis at maximum MRR condition shows rough surface finish and ovality in μ-drilled hole. Whereas high circularity and uniform drilling attributes were obtained along the whole depth at minimum OC condition.

ARTICLE HISTORY
Accepted 20 October 2022

KEYWORDS
Zn/(Ag + Fe)-MMC; stir casting; μ-drilling; ECDM; SEM

1. Introduction

Nowadays, stainless steels, titanium alloys, and cobalt-chrome alloys are mostly used in metallic implants. Despite this, their use comes with long-term risks [1–3]. As a result, biodegradable materials were developed. After serving their purpose, these materials degrade on their own after the defined function has been completed. Biodegradable materials often include magnesium, polymers and iron. These elements are also present in human diets [4–6]. The stiffness and mechanical properties of biodegradable materials make them an ideal choice for high-stress applications [7]. Zinc is an essential component of the human body, which is readily available throughout the surrounding environment. Zinc has been used for alloying in the pharmaceutical, chemical, pigment, and medical industries since ancient times. Biomedical applications are made possible by its

CONTACT Saurabh Kumar Maurya skks.saurabh@gmail.com Department of Mechanical Engineering, Punjab Engineering College (Deemed to be University), Chandigarh, India

corrosion resistance, low coefficient of friction, low melting point, and machineability [8]. Metal matrix composites (MMCs) have ductile phases reinforced by hard and brittle ceramics. MMCs are attractive due to their mechanical and physical properties. When compared with monolithic constituent components used for composite manufacturing, the composite materials exhibit superior properties [9]. MMCs based on Zinc can be effectively used as the biodegradable material [7]. Porous architecture offers the light weight structure with good mechanical properties for bio-application. Micro-drilling can be effectively used for obtaining the porous architecture. Micro holes can be produced using conventional micro-drilling process but it has rapid tool breakage and high geometrical deviation during machining of MMCs [10]. Therefore, non-conventional process such as electrical discharge machining (EDM) [11], abrasive water jet machining (AWJM) [12], laser beam machining (LBM) [13] etc. are used for producing micro holes on MMCs. But, there are some limitations associated with these processes either in the form of high equipment cost or lower MRR and dimensional accuracy.

1.1. ECDM over EDM

The electrochemical discharge machining (ECDM) and electrical discharge machining (EDM) both can be effectively used for producing μ-drill in the MMCs with high precision. In the EDM, issue like high tool wear rate and geometrical damage occur during micro drilling due to jamming of discharge gap caused by eroded particles. Also, the MRR is lower in EDM when compared to the ECDM. Jayaraj et al (2000) had compared the performance of ECDM and EDM and found that ECDM offers better machining behaviour than EDM while machining MMCs [14]. Chavoshi and Luo (2015) reviewed various hybrid micro machining processes like vibration assisted, laser assisted, fluid assisted, μ-ECM, μ-EDM, μ-ECDM and encourages to use hybrid μ-machining process (μ-ECDM) to improve surface integrity of μ-machined parts [15]. ECDM provides relatively higher MRR, smoother surface finish and lower overcut [16]. It is believed that the overall material removal mechanisms of EDM and ECDM are similar. The dominance of the discharge mechanism results in cracking in the recast layer. However, evidence for reduced energy of the ECDM spark was seen, compared to EDM, indicating that the recast layer thickness is lower for ECDM. The recast layer is almost eliminated in the case of ECDM when compared with EDM [15,17,18]. Paul and Hiremath (2016) had reviewed theoretical and experimental aspects of ECDM focusing on output parameters like MRR, heat affected zone (HAZ), TWR. Study deals with in-depth analysis of input parameters like pulse duration, voltage, current, and feed rate on machining of non-conductive materials. Authors claimed that ECDM has immense potential over EDM and ECM to machine engineering materials with higher accuracy and precision [19].

1.2. Literature review on ECDM

ECDM combines the effect of both electrical discharge machining (EDM) and electro-chemical machining (ECM) for removal of material [20]. In the ECDM material removal takes place due to electro-spark erosion, while electrochemical dissolution provides a smooth surface to the workpiece [21,22]. ECDM was found effective for creating

micro groove, holes and slots [23,24]. Molds and dies can also be resurfaced using the ECDM to remove large surfaces irregularities that have been left after milling [25]. advanced ceramic materials can also be effectively machined by ECDM process [26,27]. The selection of significant machining process parameter and their range during micro-drilling are crucial for enhancing MRR, surface quality and tool life [28,29]. This improves the tool cost and enhances surface superiority when the right parameters and conditions are chosen [30,31]. In ECDM electrochemical reaction rate, gas film formation, and discharge characteristics are all affected by the process variables. Variations in magnitude of the different process variables can drastically alter a process overall mechanism [32].

Doloi et al. (1997), Bhattacharyya et al. (1997) and Doloi et al. (1998) analysed the effects of process variables on MRR and OC while performing ECDM on ceramics and found that MRR increased as supplied voltage and concentration of NaOH in electrolyte solution increased. The overcut was also increased as electrolyte concentration increased. They also conclude that ECDM can be effectively used to drill small holes with extreme degree of precision [33–35]. Pramanik (2014) has studied the effect of feed rate, electrolyte concentration, applied voltage, pulse-on-time, pulse-off-time, current and intermediate gap on MRR during ECDM of MMCs. Author concluded that MRR increases as applied voltage, feed rate and electrolyte concentration increase. Author found that pulse duration, applied current voltage and electrolyte concentration are major factor for increasing MRR. Low pulse-on-time and low feed rate leads to decrease overcut and surface roughness of MMC [36]. Manna and Malik (2016) had investigated the effect of supply voltage, electrolyte type and electrolyte concentration during μ-drilling of Al-MMC on developed ECMM setup. Studied was limited to investigation of MRR and overcut. Authors claimed increase in MRR and overcut with increase in electrolyte concentration taking mixed electrolyte type [37]. Madhavi and Hiremath (2016) investigated μ-channelling and μ-holes of borosilicate and soda-lime glass utilising μ ECDM. Design of Experiments was used to optimise voltage and electrolyte concentration for MRR, TWR and radial overcut (ROC). It has been found that with increase in voltage and electrolyte concentration MRR, ROC, TWR increases. Controlled voltage supply resulted in minimising TWR and ROC [38]. Singh and Dvivedi found that supply voltage, pulse-on-time, pulse-off-time and electrolyte concentration have significant effect on the MRR, radial overcut during machining of borosilicate glass using ECDM [32,39]. Paul et al. (2021) found supply voltage has highest influence on the MRR and radial overcut when compared to the electrolyte concentration and duty factor while micro machining of borosilicate glass utilizing ECDM [40]. Rajput et al. (2021) found that supply voltage, electrolyte concentration have significant effect on MRR and tool wear rate while machining soda line glass utilizing ECDM [41]. Totabi and Razfar (2021) proposed effective μ-channeling of PDMS utilizing ECDM. Authors studied the effect of tool diameter and type of electrolyte solution on dimensional accuracy, material removal rate and surface quality of μ-channels. Electrolyte concentration was maintained at 25% and NaOH, KOH electrolyte type with varying temperature were investigated. It has been observed that with decreasing tool diameter, lower surface roughness has been achieved. It has also been claimed by authors that NaOH resulted in lower surface roughness width, while more material removal [42].

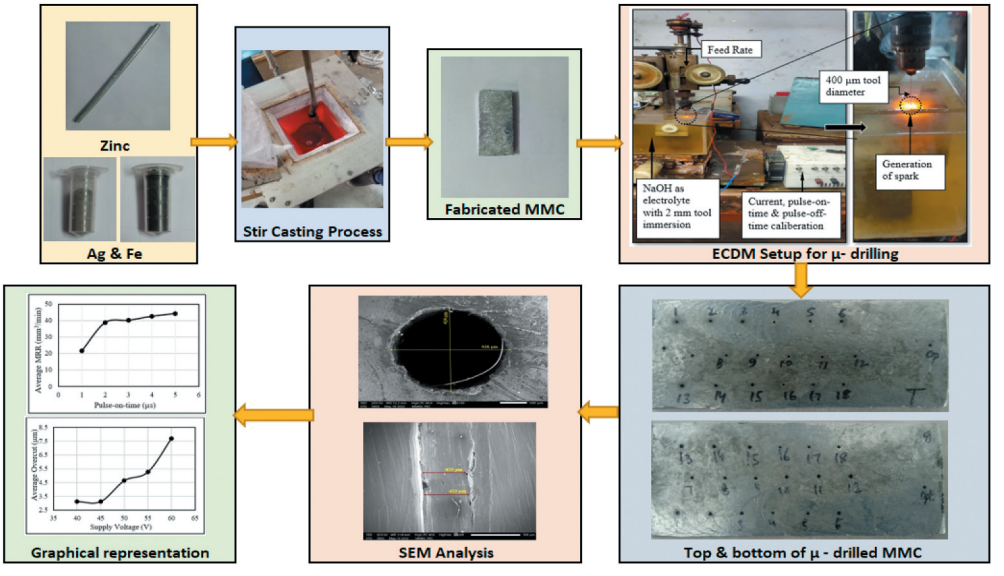

Figure 1. Flow diagram of the work performed during current study.

From the study, it was found that there is very less available literature on fabrication of Zn MMCs. Also, most of the research on micro drilling utilising ECDM was carried out either on the ceramics or on glass; however, no studies have been found on µ-drilling of zinc based MMCs. Therefore, in the present study, fabrication of Zn/(Ag + Fe)-MMCs was done using stir casting method and an experimental investigation is performed during µ-drilling on Zn/(Ag + Fe)-MMCs specimen utilizing electrochemical discharge machining set-up. Based on the literature review, ECDM process parameters such as supply voltage, peak current, pulse-on-time, pulse-off-time, feed rate and electrolyte concentration taken as input variables, whereas MRR, OC and TW were taken as output responses. The main objective of current research is to identify the effect of ECDM parameters on machining response characteristics during machining of such MMCs. Various effects plots were used to analyse the test results, and a range of values for each-individual parameter was determined to be most effective for machining of new hybrid Zn/(Ag + Fe)-MMC. The SEM analysis of machined surfaces were performed to explore the surface texture generated after µ-drilling on Zn/(Ag + Fe)-MMC. Figure 1 shows the flow diagram of entire research work performed during current experimental investigation.

2. Fabrication of hybrid Zn/(Ag + Fe)-MMC

For the fabrication of hybrid Zn/(Ag + Fe)-MMC, liquid stir casting method was employed [7,43]. Liquid stir casting method had proved to be simple and low-cost compared to other processes used to fabricate hybrid MMCs [44,45]. For the fabrication of hybrid Zn/(Ag + Fe)-MMC, Zn was used as matrix phase and 1 wt % silver (Ag) & 1 wt % iron (Fe) nanoparticles with an average particle size of 150 nm were used as

reinforcement materials. In order to conduct the further experimental investigation, workpieces with dimensions of 80 mm x 32 mm x 6 mm were fabricated.

The microscopic structure of the hybrid Zn/(Ag + Fe)-MMC was examined using optical microscopy (Radical Scientific Equipment Model-RXLr-4 M –7001-10N, Sr. No. CC-110) and shown in Figure 2 (a). From Figure 2(a), it is possible to observe the grain boundaries which show that particles are uniformly distributed with some cluster formations. Some dark spots in Figure 2(a) confirm the presence of reinforced particles in the fabricated MMC. A significant accumulation of Fe particles surrounds the Ag particles. Clear zinc dendritic formations can also be seen in the figure. SEM analysis (JEOL JSM-IT500 LV, Japan) of fabricated hybrid Zn/(Ag + Fe)-MMC specimen is illustrated in Figure 2(b). In Figure 2(b), the base material (Zn) appears in the dark grey areas, whereas Ag particles are found in the black areas. The Fe particles were found in the vicinity of Ag particles depicting whitish shade. The elemental composition of fabricated MMC was determined using energy dispersive spectroscopy (EDS, Oxford instruments ultim max, UK). In Figure 2(c), the EDS maps of fabricated Zn/(Ag + Fe)-

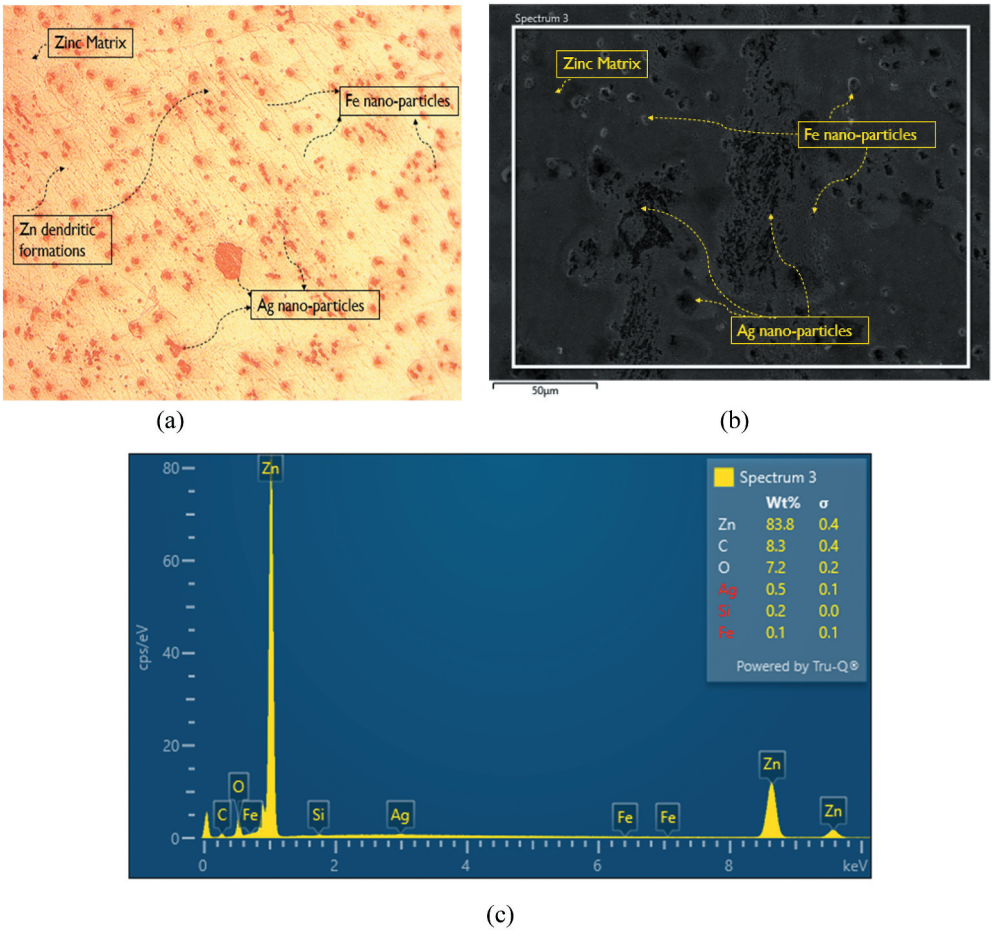

Figure 2. (a) Optical microscopy; (b) SEM; (c) EDS of fabricated novel hybrid Zn/(Ag + Fe)-MMC sample.

Table 1. Mechanical properties of fabricated hybrid Zn/(Ag + Fe)-MMC.

Mechanical properties	Zn/(Ag + Fe)-MMC
Density (g/cc)	6.805
Ultimate tensile strength (MPa)	180.3
Yield strength (MPa)	157.67
Percentage elongation	38 %
Microhardness (hv)	51.82

MMC samples reveal the presence of all the elements. Mechanical properties of fabricated Zn/(Ag + Fe)-MMC sample were also evaluated using universal testing machine (UTE 40 HGFL Sr.No. 1/2017–5826) & Vickers microhardness tester (HV1000B HUAY IN, Sr. No. 0012) and given in Table 1.

3. Planning for experimentation

For identifying the effect of individual process variables on the response characteristics, experiments were performed based on one factor at a time approach i.e. one process variable is varied while other variables kept constant at their mid value. This type of experimental investigation also recognises as pilot experiments or preliminary experiments. To reduce the amount of time and cost of experiments, it is necessary to carry out preliminary experiments before conducting large-scale quantitative analyses. Table 2 shows the design of experiments used for performing preliminary experiments. For present experimental investigation supply voltage, peak current, pulse-on-time, pulse-off-time, feed rate, electrolyte concentration was selected as process variable and material removal rate (MRR), overcut (OC), tool wear (TW) were selected as output responses for μ-drilling of hybrid Zn/(Ag + Fe)-MMC using ECDM.

A series of μ-drilling experiments were performed on the fabricated ECDM set-up shown in Figure 3. Stir casted hybrid Zn/(Ag + Fe)-MMC of size 80 mm x 32 mm x 6 mm was used as workpiece material and a brass wire of 400 μm diameter was used as tool electrode. In order to perform machining operations, the negative terminal of the power supply was connected to the tool electrode and the positive terminal was connected to the workpiece specimen. A list of the ECDM parameters and their settings used for experiments are shown in Table 2. Each experiment was replicated three times and the average results were taken for plotting the effect graph of individual process variables on response characteristics. Table 3 shows the average result of output response for individual parametric setting.

3.1. Estimation of MRR, OC and TWR

The material removal rate (MRR) was estimated by calculating the volume of material extracted from workpiece after drilling. The tool wear (TW) was measured by change in weight of the tool before and after each micro-drill [41]. The overcut (OC) was measured by taking the difference between drilled hole diameter and tool diameter [46]. The following relations were used to estimate the MRR, OC and TW respectively.

Table 2. Parametric level and their settings considered for experiments on ECDM.

Stages of Experiments	Ex. No.	Parameters and variation of their setting values					
		Supply Voltage (V)	Peak Current (A)	Pulse-on-time (μs)	Pulse-off-time (μs)	Feed rate (mm/min)	Electrolyte conc. (wt. %)
Stage-I (Varying supply voltage)	1	40	Constant Peak current = 3 A	Constant Pulse-on-time = 3 μs	Constant Pulse-off-time = 3 μs	Constant feed rate = 30 mm/min	Constant electrolyte concn. = 20 wt. %
	2	45					
	3	50					
	4	55					
	5	60					
Stage-II (Varying Peak current)	6	Constant Supply Voltage = 50 V	1	Constant Pulse-on-time = 3 μs	Constant Pulse-off-time = 3 μs	Constant feed rate = 30 mm/min	Constant electrolyte concn. = 20 wt. %
	7		2				
	8		3				
	9		4				
	10		5				
Stage-III (Varying Pulse-on-time)	11	Constant Supply Voltage = 50 V	Constant Peak current = 3 A	1	Constant Pulse-off-time = 3 μs	Constant feed rate = 30 mm/min	Constant electrolyte concn. = 20 wt. %
	12			2			
	13			3			
	14			4			
	15			5			
Stage-IV (Varying Pulse-off-time)	16	Constant Supply Voltage = 50 V	Constant Peak current = 3 A	Constant Pulse-on-time = 3 μs	1	Constant feed rate = 30 mm/min	Constant electrolyte concn. = 20 wt. %
	17				2		
	18				3		
	19				4		
	20				5		
Stage-V (Varying feed rate)	21	Constant Supply Voltage = 50 V	Constant Peak current = 3 A	Constant Pulse-on-time = 3 μs	Constant Pulse-off-time = 3 μs	10	Constant electrolyte concn. = 20 wt. %
	22					20	
	23					30	
	24					40	
	25					50	
Stage-VI (Varying electrolyte concentration)	26	Constant Supply Voltage = 50 V	Constant Peak current = 3 A	Constant Pulse-on-time = 3 μs	Constant Pulse-off-time = 3 μs	Constant feed rate = 30 mm/min	10
	27						15
	28						20
	29						25
	30						30

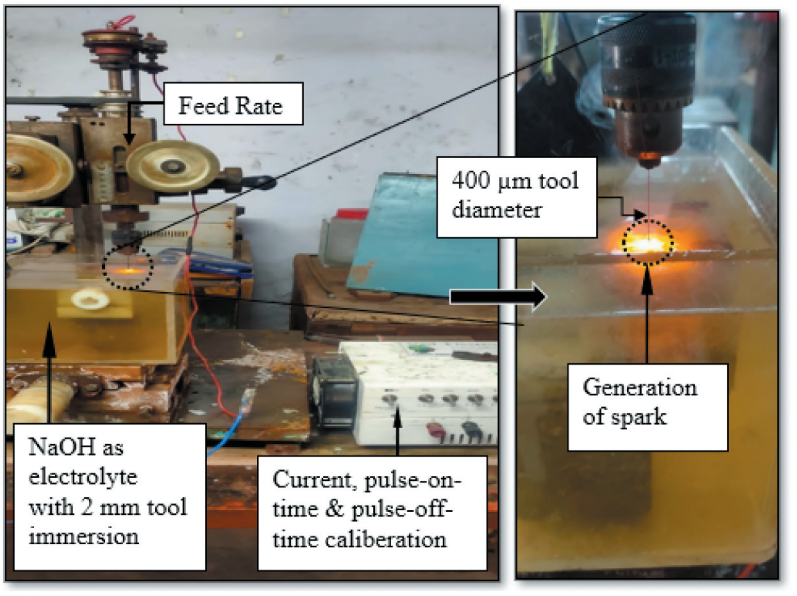

Figure 3. Fabricated ECDM set-up used for µ-drilling of hybrid Zn/(Ag + Fe)-MMC specimen.

$$\mathrm{MRR}(mm^3/min) = \frac{\pi T}{12t}\left[\frac{D_i^3 - D_b^3}{D_b}\right]\mathrm{x}1000 \qquad \text{Eqn.1}$$

$$\mathrm{OC}(\mu m) = \mathrm{Dtool} - \left(\frac{\mathrm{Dt} + \mathrm{Db}}{2}\right) \qquad \text{Eqn.2}$$

$$\mathrm{TW}\ (mg) = \mathrm{W_i} - \mathrm{W_f} \qquad \text{Eqn.3}$$

Where, W_i is initial weight, W_f is final weight, t represents the continuous machining time in minutes, T represents the thickness of fabricated Zn/(Ag + Fe)-MMC. D_{tool} is tool diameter, D_t is top machined diameter and D_b is bottom machined diameter. D_t and D_b are measured using stereo microscope.

4. Result and discussion

A total of 30 µ-drilling experiments with three replications were performed using ECDM set-up on fabricated novel hybrid Zn/(Ag + Fe)-MMC specimens. The average values of responses given in Table 3 (MRR, OC, TW) are used to plot the various effect graphs. Detailed study of the effect of each process variable on the responses is described in following articles.

Table 3. Average results of the output responses.

Stages of experiments	Ex. No.	Average MRR (mm^3/min)	Average OC (μm)	Average TW (mg)
Stage-I (Varying supply voltage)	1	19.501	3.12	0.0072
	2	28.38	3.124	0.01321
	3	35.71	4.64	0.01548
	4	47.093	5.265	0.01622
	5	59.19	7.696	0.019786
Stage-II (Varying Peak current)	6	21.62	1.97	0.0072
	7	24.78	2.57	0.0112
	8	29.15	2.88	0.0197
	9	37.89	2.96	0.02561
	10	42.064	3.83	0.02843
Stage-III (Varying Pulse-on-time)	11	21.59	3.81	0.00723
	12	38.76	3.84	0.009801
	13	40.17	3.98	0.00139
	14	42.58	4.179	0.001265
	15	44.28	4.263	0.01012
Stage-IV (Varying Pulse-off-time)	16	39.10	6.993	0.0287
	17	33	6.481	0.0204
	18	29.03	3.601	0.0153
	19	21.02	2.86	0.0106
	20	16.97	1.62	0.00721
Stage-V (Varying feed rate)	21	20.01	7.84	0.00719
	22	32	6.803	0.0096
	23	52.96	5.97	0.0114
	24	73.13	5.54	0.0119
	25	81	4.83	0.0134
Stage-VI (Varying electrolyte concentration)	26	14.71	2.33	0.0072
	27	18	2.18	0.0093
	28	20.30	3.87	0.01335
	29	26.3	6.89	0.01516
	30	29.50	7.91	0.01921

4.1. Effect of process variables on MRR

Figure 4 shows the effect of process variables such as supply voltage, peak current, pulse-on-time, pulse-off-time, feed rate and electrolyte concentration on MRR. Figure 4(a,b) illustrates that, MRR increases as supply voltage and peak current increases. The sparks were formed between tool electrode and electrolyte only when the potential difference between them is sufficient. An increase in the supply voltage and peak current may cause the development of high thermal energy, which results in formation of higher number of large gas bubbles. The sparks travel through these gas bubbles. It causes a high-velocity stream of electrons to flow from the electrode to the workpiece rapidly with tremendous acceleration. Due to this workpiece surfaces get melted, vaporised and thermally eroded which ultimately increases the MRR [47,48]. The supply voltage was found to be significant process variables for MRR during ECDM process [49]. From Figure 4(c), it is clear that the MRR increases with increase in pulse-on-time. There is a direct correlation between pulse duration and spark generation. As pulse-on-time increases, the heat flux on the workpiece as well as dissolution efficiency increases which results an increase in MRR. Figure 4(d) shows that MRR decreases as pulse-off-time increases. At high pulse-off-time, more time is available for the cooling of electrode and workpiece. Therefore, the temperature generated during the machining process will be lower and it will not be sufficient to remove higher material by electrochemical dissolution.

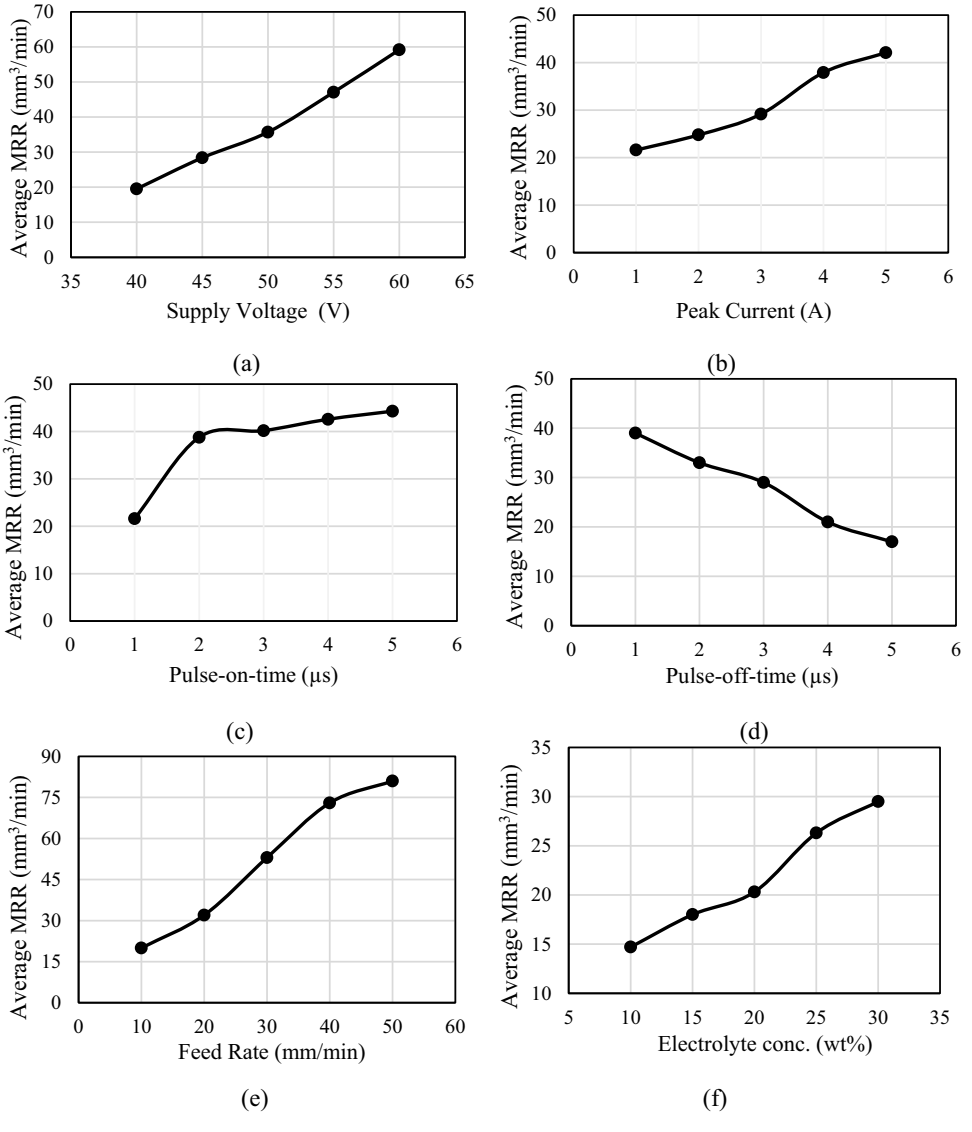

Figure 4. Effect of (a) supply voltage, (b) peak current, (c) pulse-on-time, (d) pulse-off-time, (e) feed rate and (f) electrolyte concentration, on MRR.

Figure 4(e) shows that MRR is also increases as the feed rate increases. It is due to increase in the cutting force. From Figure 4(f) it is clear that MRR increases with increase in electrolyte concentration due to increment in thermal energy. Thermal energy produced during ECDM directly depends on electrolyte concentration [50]. Concentration of hydroxyl (OH-) ions also increases with electrolyte concentration [51]. Electrolyte concentration was found to be important process variable for determination of MRR during ECDM [52].

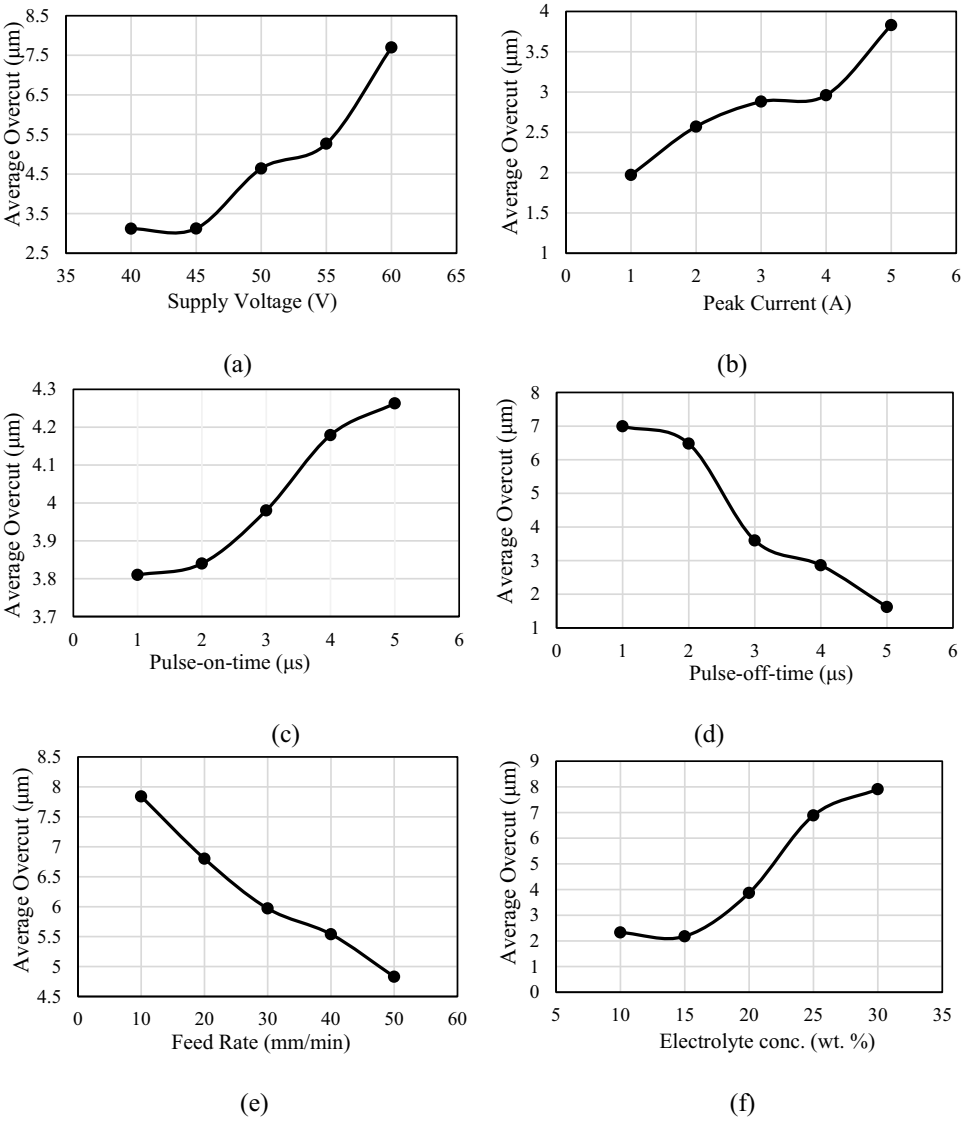

Figure 5. Effect of (a) supply voltage, (b) peak current, (c) pulse-on-time, (d) pulse-off-time, (e) feed rate and (f) wt. % electrolyte concentration, on overcut.

4.2. Effect of process variables on overcut

Figure 5 shows the effect of process variables such as supply voltage, peak current, pulse-on-time, pulse-off-time, feed rate and wt. % of electrolyte concentration on overcut. From Figure 5(a) and Figure 5(b), it was observed that with an increase in supply voltage and peak current overcut increases. As supply voltage and peak current increases larger number of gas bubbles generated due to higher thermal energy which causes a high-velocity stream of electrons to flow from the electrode to the workpiece. Hence, higher melting, vaporisation and erosion of workpiece increases the overcut. The effect of pulse-on-time on overcut is shown by Figure 5(c). It can be seen that,

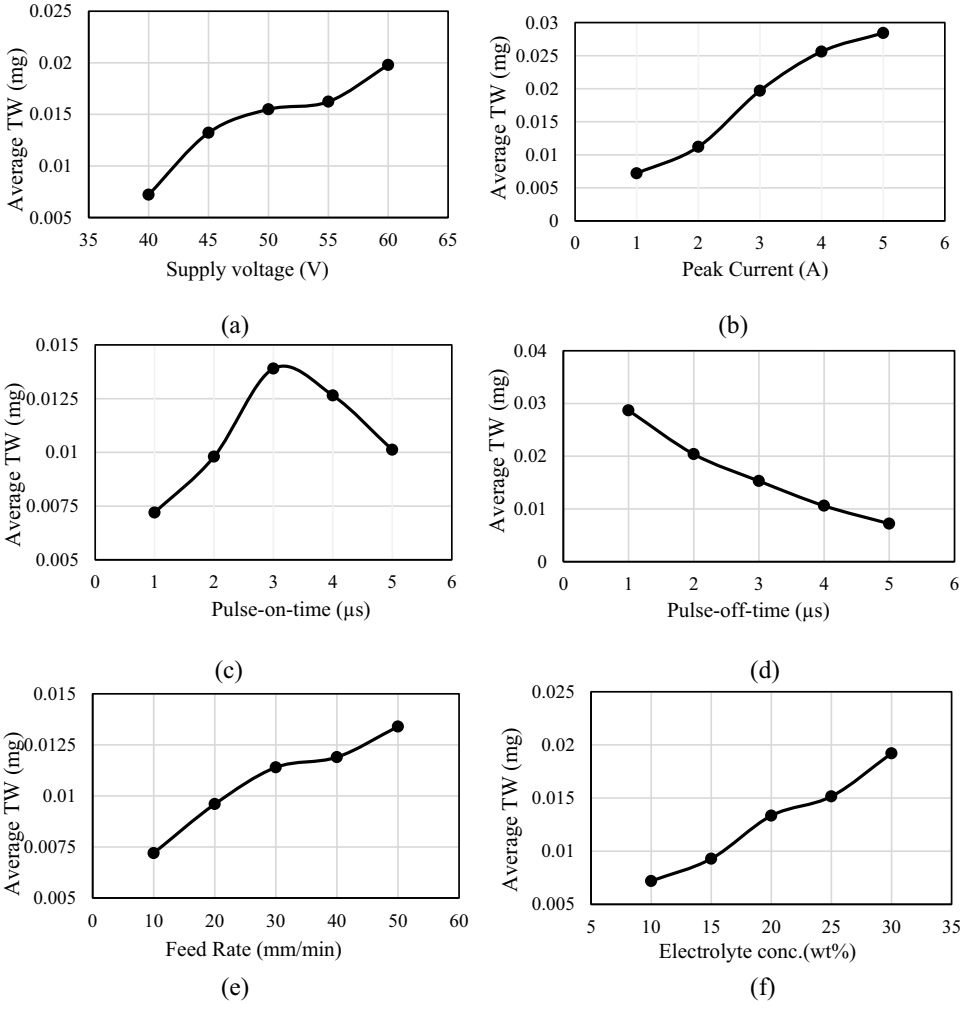

Figure 6. Effect of (a) supply voltage, (b) peak current, (c) pulse-on-time, (d) pulse-off-time, (e) feed rate and (f) electrolyte concentration, on TW.

overcut increases with a slower rate in the range of 1 µs to 3 µs pulse-on-time when compared to the 3 µs to 5 µs pulse-on-time. The thin gas films generated from the micro-cavities of electrode at lower pulse-on-time when compared to the higher pulse-on time. It leads to the low-intensity discharges due to the breakdown of thin gas films. Consequentially, the electrode only liberates a small amount of energy during ECDM, it results in a small overcut. By extending the pulse-on-time (3 µs to 5 µs), the gas bubbles are accumulated at the electrode for longer periods of time, resulting in thicker gas film formation and produce high-intensity discharges. Due to this excess thermal energy liberated at the machining zone and higher overcut occur [53]. While, on reverse, with increasing pulse-off-time, overcut decreases as shown in Figure 5(d,e). shows that overcut decreases as feed rate increases because increasing the feed rate provide insufficient time for thermal energy to be released for material removal. An

increment in the feed rate results very small cavities between the tool electrode and the work material. It produces small energy at the machining zone which utilised for surface heating of the work material. No melting or evaporation takes place due to this energy.

From the Figure 5 (f), it was observed that with an increase in electrolyte concentration overcut increases. Low electrolyte concentration during ECDM results insufficient thermal energy to remove the material from the workpiece. As most of the thermal energy used to increase the temperature of the work material. On increasing the electrolyte concentration, increases the hydroxyl (OH-) ions which increases the thermal energy produced during ECDM. This excess thermal energy is the reason for increased overcut [54,55].

4.3. Effect of process variables on TW

Figure 6 shows the effect of process variables such as supply voltage, peak current, pulse-on-time, pulse-off-time, feed rate and wt. % of electrolyte concentration on TW. From Figure 6(a,b) it is clear that as supply voltage and peak current increase tool wear increases. An increase in supply voltage and peak current leads to the generation of strong sparks between the tool and the workpiece. It leads to the higher temperature between the tool and the workpiece, which improves the melting and evaporation rates and increases tool wear. Chemical reactions occur between electrolyte and tool electrode at high temperature can also cause the tool wear. It can be seen from Figure 6(c) that up to a pulse-on-time of 3 μs, TW increases, but beyond that, it decreases as pulse-on-time increases. As the pulse-on-time increases, thermal energy also increases due to spark generated for longer time. It increases the tool wear initially. On further increasing the pulse-on-time, more melting of material takes place and act as the barrier for the flow of sparks which ultimately slows down the TW. From Figure 6(d) it is clear that increasing pulse-off-time tool wear decreases. Higher pulse-off-time provides time lapse in generation of spark, allowing tool to cool down and leading to less tool wear. Even though there is no mechanical wear due to friction, compression shock waves may cause tool wear during sparking. The workpiece material may undergo the positive ionisation when heated to a high temperature. It leads to the formation of gas bubbles due to electrochemical reactions. By connecting auxiliary electrodes to direct current power sources, the electrode materials are likely to be positively ionised. In ECDM, positive ions strike the tool surface with less momentum, causing lower tool wear but tools wear more rapidly when they function as anodes, as more heat is absorbed by the anodes during arcing. As the feed rate increases, additional wear on the tool caused by the formation of gas bubbles and positively ionized particles increases as shown in Figure 6(e). The spark energy in the electrolyte increases as voltage and specific conductivity of the electrolyte increase, resulting in increased tool wear which can be depicted from Figure 6(f).

5. Analysis of machined surface

The application of any machined surface delicately depends upon the surface texture obtained by particular machining process. Texture of machined surface differentiates the effective processes that can be used for machining. The analysis of machined surface can be effectively done by taking the scanning electrode microscopic

images using JEOL JSM-IT500 LV, Japan SEM machine. Figure 7 shows the SEM images of μ-drilled machined surface texture. Figure 7a shows the SEM image of machined hole corresponding to the combination of process variables for which MRR was minimum i.e. 40 V supply voltage, 1 A peak current, 1 μs pulse-on-time, 5 μs pulse-off-time, 10 mm/min feed rate and 10 % electrolyte (Figure 4). Figure 7b shows cross-sectional view of μ-drilled hole at same process variable setting. The measured dimensions of hole confirm the low circular dimensions. The MRR is comparatively low due to lower value supply voltage, peak current, pulse-on-time, feed rate and electrolyte concentration. Figure 7c shows the SEM image machined hole corresponding to the combination of process variables for which MRR is maximum i.e. 60 V supply voltage, 5 A peak current, 5 μs pulse-on-time, 1 μs pulse-off-time, 50 mm/min feed rate and 30 % electrolyte concentration. Figure 7d shows cross-sectional view of μ-drilled hole at same process variable setting. From the Figure 7c it is

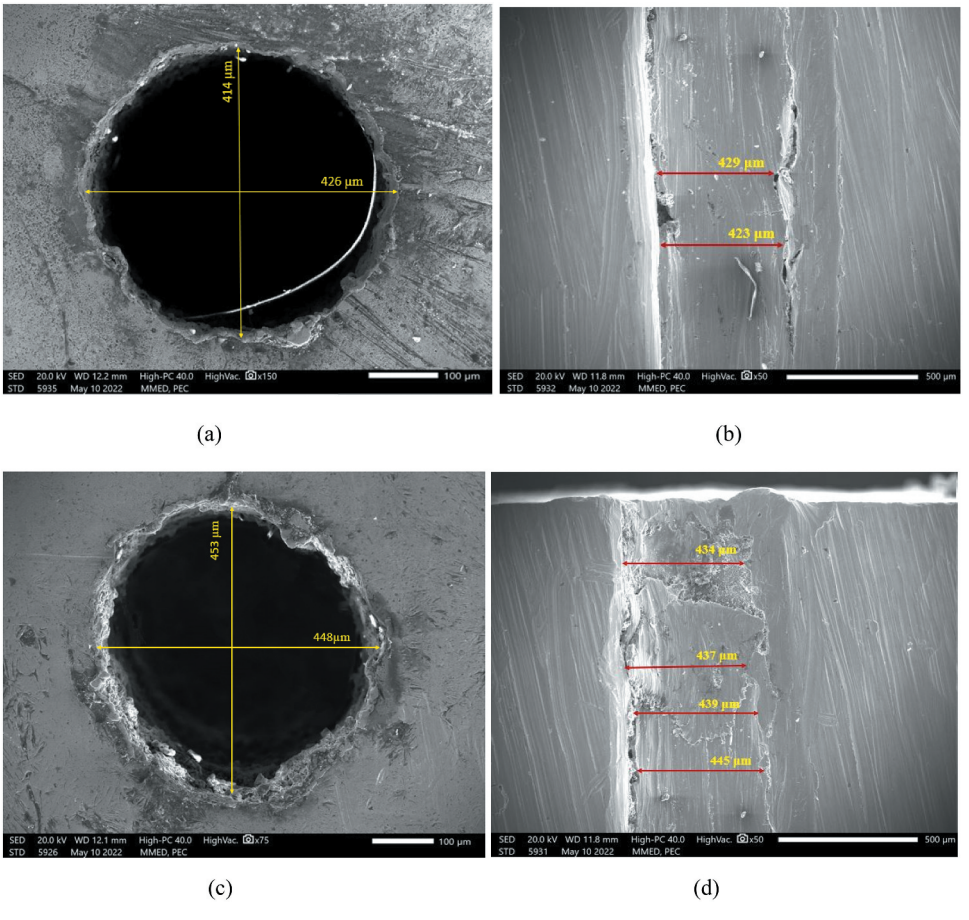

Figure 7a. SEM image of μ-drilled hole on novel hybrid Zn/ (Ag + Fe)-MMC depicting at processvariables combination for (a) minimum MRR; (b) cross-sectional view for minimum MRR (c) maximum MRR; (d) cross-sectional view for maximum MRR; (e) maximum OC; (f) cross-sectional view formaximum OC (g) minimum OC; (h) cross-sectional view for minimum OC.

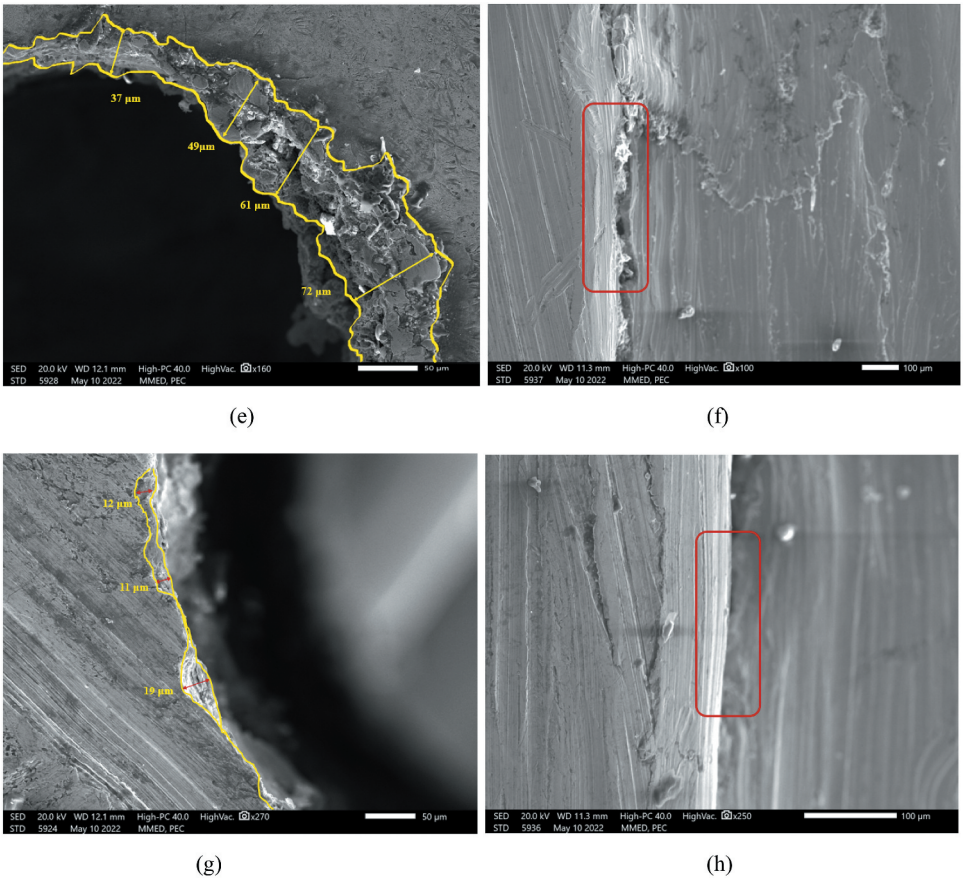

Figure 7b. SEM image of µ-drilled hole on novel hybrid Zn/ (Ag + Fe)-MMC depicting at process variables combination for (a) minimum MRR; (b) cross-sectional view for minimum MRR (c) maximum MRR; (d) cross-sectional view for maximum MRR; (e) maximum OC; (f) cross-sectional view for maximum OC (g) minimum OC; (h) cross-sectional view for minimum OC.

clear that, machined surface has oval shape and measured dimensions of hole using ImageJ software confirm the ovality in µ-drilled hole. However, the inside surface of machined hole can get affected by heat affected zone formed due to interrupted sparking during machining. This interrupted sparking occurs due to high or improper feed rate and inadequate current supply. Micro hole drilling produces rough surfaces, which may cause sparks to spread irregularly over a wide area. In addition, molecules and ions also removed irregularly from the surface of the hole which can be seen in Figure 7d. This condition of high feed rate, high pulse-on-time, and high supply voltage also tends to maximum overcut as shown in Figure 7e and Figure 7f. Larger overcut occurs as a result of excess thermal energy being liberated at the machining zone due to high-intensity discharges. It is also validated from the SEM analysis that overcut having maximum width of 72 µm. Burrs, fin formations and abrupt finished surfaces are also visible along the whole depth of machined surface and can be seen in Figure 7f.

Figure 7g shows the SEM image of machined hole corresponding to the combination of process variables for which overcut is minimum i.e. 40 V supply voltage, 1 A peak current, 1 µs pulse-on-time, 5 µs pulse-off-time, 50 mm/min feed rate and 15 % electrolyte concentration. Figure 7h shows cross-sectional view of µ-drilled hole at same process variable setting. From Figure 7g, high circularity and less overcut of µ-drilled surface can be clearly seen. It is because of low thermal energy being liberated at the machining zone due to low supply voltage, current, pulse-on-time & electrolyte concentration and high feed rate & pulse-off-time. It is validated from Figure 7g that overcut having maximum width of 19 µm. Also, at some places less than 5 µm of overcut can be seen. Additionally, uniform drilling attributes are visible along the whole depth of machined hole and can be seen in Figure 7h.

6. Conclusions

The research presents the fabrication of novel Zn/(Ag + Fe)-MMC employing the stir casting method. Microstructural and mechanical properties of fabricated MMC were identified. The fabricated Zn/(Ag + Fe)-MMC can be used for the biomedical application such as cardiovascular stents. ECDM was employed for the µ-drilling on fabricated Zn/(Ag + Fe)-MMC specimens for making porous architecture. The effect of different process variables such as supply voltage, pulse-on-time, pulse-off-time, feed rate and electrolyte concentration were analysed on MRR, OC and TW using one-factor-at-time approach. From the experimental investigation following conclusion can be drawn out:

(i) The uniform distribution of reinforced particles in Zn/(Ag + Fe)-MMC reveals that stir casting method can be used for the fabrication of such MMCs.
(ii) ECDM process can be effectively used to produce highly accurate µ-size holes on newly fabricated hybrid Zn/(Ag + Fe)-MMC.
(iii) It was found that MRR increases as supply voltage, peak current, pulse-on-time, feed rate, electrolyte concentration increase and decreases as pulse-off-time increases.
(iv) Overcut was found to be increased with supply voltage, peak current and pulse-on-time whereas decreases with increase in pulse-off-time and feed rate. Minimum OC was observed at 15 wt % electrolyte concentration.
(v) TW increases as supply voltage, peak current, feed rate and electrolyte concentration increase. For pulse-on-time, TW initially increases up-to 3 µs and then decreases as pulse-on-time further increases.
(vi) SEM image taken at the process variable combination for maximum MRR shows the rough surface and ovality in the µ-drilled hole. Whereas SEM image taken for minimum overcut confirms the uniformity in drilled hole along the whole depth. Additionally, high circularity was obtained at minimum OC condition.

The experimental investigation was performed using fixed composition of the Ag and Fe reinforcement in Zn/(Ag + Fe)-MMC. Further experimental investigation needs to be performed using different composition of Ag and Fe in Zn/(Ag + Fe)-MMC for better results and application.

Disclosure statement

No potential conflict of interest was reported by the author(s).

ORCID

Saurabh Kumar Maurya http://orcid.org/0000-0002-1048-3961

References

[1] Rodrigues WC, Broilo LR, Schaeffer L, et al. Powder metallurgical processing of Co–28% Cr–6% Mo for dental implants: physical, mechanical and electrochemical properties. Powder Technol. 2011;206(3):233–238.
[2] Gepreel MAH, Niinomi M. Biocompatibility of Ti-alloys for longterm implantation. J Mech Behav Biomed Mater. 2013;20:407–415.
[3] Subramanian B, Ananthakumar R, Kobayashi A, et al. Surface modification of 316L stainless steel with magnetron sputtered TiN/VN nanoscale multilayers for bio implant applications. J Mater Sci. 2012;23(2):329–338.
[4] Lin W, Qin L, Qi H, et al. Long-term in vivo corrosion behavior, biocompatibility and bioresorption mechanism of a bioresorbable nitrided iron scaffold. Acta Biomater. 2017;54:454–468.
[5] Virtanen S. Biodegradable Mg and Mg alloys: corrosion and biocompatibility. Mater Sci Eng B. 2011;176(20):1600–1608.
[6] Nair LS, Laurencin CT. Biodegradable polymers as biomaterials. Progress Polym Sci. 2007;32(8–9):762–798.
[7] Guan Z, Pan S, Linsley C, et al. Manufacturing and characterization of Zn-WC as potential biodegradable material. Procedia Manuf. 2019;34:247–251.
[8] Zhou P, Erning JW, Ogle K. Interactions between elemental components during the dealloying of Cu-Zn alloys. Electrochim Acta. 2019;293:290–298.
[9] Antil P, Singh S, Manna A. Effect of reinforced SiC particulates of different grit size on mechanical and tribological properties of hybrid polymer matrix composites. Mater Today Proc. 2018;5(2):8073–8079.
[10] Khadtare A, Pawade R, Varghese A, et al. Micro-drilling of straight and inclined holes on thermal barrier coated Inconel 718 for turbine blade cooling. Mater Manuf Processes. 2020;35(7):783–796.
[11] Singh MA, Rajbongshi SK, Sarma DK, et al. Surface and porous recast layer analysis in μ-EDM of MWCNT-Al2O3 composites. Mater Manuf Processes. 2019;34(5):567–579.
[12] Liu D, Nguyen T, Wang J, et al. Mechanisms of enhancing the machining performance in micro abrasive waterjet drilling of hard and brittle materials by vibration assistance. Int J Mach Tools Manuf. 2020;151:103528.
[13] Wang C, Xue S, Chen G, et al. Influence of laser parameters on micro-hole drilling of Cu50Zr50 amorphous alloys foil. Ferroelectrics. 2018;523(1):61–67.
[14] Jayaraj J, Mahal A, Ravi S, et al. Electrochemical discharge machining of Al-SiC Composites. Proceedings of the Int. Conf. on Manufacturing, ICM 2000, BUET, Dhaka (Bangladesh). 2000;257–265.
[15] Chavoshi SZ, Luo X. Hybrid micro-machining processes: a review. Precis Eng. 2015;41:1–23.
[16] Gupta PK, Dvivedi A, Kumar P. Effect of pulse duration on quality characteristics of blind hole drilled in glass by ECDM. Mater Manuf Process. 2015;31(13):1740–1748.
[17] Liao Z, la Monaca A, Murray J, et al. Surface integrity in metal machining-Part I: fundamentals of surface characteristics and formation mechanisms. Int J Mach Tools Manuf. 2021;162:103687.

[18] Xu Z, Zhang C. A tube electrode high-speed electrochemical discharge drilling method without recast layer. Procedia CIRP. 2018;68:778–782.
[19] Paul L, Hiremath SS. Experimental and theoretical investigations in ECDM Process – an Overview. Procedia Technol. 2016;25:1242–1249.
[20] Kumar N, Mandal N, Das AK. Microelectrochemical sparks machining: a modern approach for fabrication of micro-components from nonconductive materials. In: Micro electro-fabrication. ELsevier. 2021. pp. 277–315.
[21] Wuthrich R, AbouZiki JD. Micromachining using electrochemical discharge phenomenon fundamentals and application of spark assisted chemical engraving. 2nd ed. William Andrew: Elsevier; 2014.
[22] Singh M, Singh S, Kumar S. Environmental aspects of various electrolytes used in electro-chemical discharge machining process. J Braz Soc Mech Sci Eng. 2020;42(8):395.
[23] Kolhekar KR, Sundaram M. A study on the effect of electrolyte concentration on surface integrity in micro electrochemical discharge machining. Procedia CIRP. 2016;45:355–358.
[24] Ghoshal B, Bhattacharyya B. Electrochemical micromachining of microchannel using optimum scan feed rate. J Manuf Processes. 2016;23:258–268.
[25] Changjian L, An G, Meng L, et al. The micro-milling machining of pyrex glass using the electrochemical discharge machining process. Adv Mater Res. 2012;403:738–742.
[26] Ladeesh VG, Manu R. Performance evaluation and multi-response optimization of grinding-aided electrochemical discharge drilling (G-ECDD) of borosilicate glass. J Braz Soc Mech Sci Eng. 2018;40(12):568.
[27] Sorkhel SK, Bhattacharyya B, Mitra S, et al. Development of electrochemical discharge machining of advanced ceramics. International Conference on Agile Manufacturing, Bangalore (India). 22-24 February1996.
[28] Ladeesh VG, Manu R. Grinding aided electrochemical discharge drilling (G-ECDD): a theoretical analysis and mathematical modelling of material removal rate. J Braz Soc Mech Sci Eng. 2021;43(9):422.
[29] Chen MJ, Ni HB, Wang ZJ. Research on the modeling of burr formation process in micro-ball end milling operation on Ti–6Al–4V. Int J Adv Manuf Technol. 2012;62(9–12):901–912.
[30] Pradeep N, Sundaram KS, Kumar MP. Multi-response optimization of electrochemical micromachining parameters for SS304 using polymer graphite electrode with $NaNO_3$ electrolyte based on TOPSIS technique. J Braz Soc Mech Sci Eng. 2019;41(8):323.
[31] Carou D, Rubio EM, Herrera J, et al. Latest advances in the micro-milling of titanium alloys: a review. Procedia Manuf. 2017;13:275–282.
[32] Singh T, Dvivedi A. A pressurized feeding approach for effective control on working gap in ECDM of borosilicate glass. Mater Manuf Processes. 2018;33(4):462–473.
[33] Doloi B, Kumar S, Mitra S, et al. Analysis of the Electrochemical Discharge Machining (ECDM) system for machining ceramics. 17th AIMTDR, REC Warangal January 9-111997:295–299.
[34] Bhattacharyya B, Doloi B, Mitra S, et al. Experimental analysis on the Electrochemical Discharge Machining (ECDM) system for advanced ceramics. In: Int. Conf. on Precision Engg. ICPE, Taipei, Taiwan. 1997. pp. 715–720.
[35] Doloi B, Bhattacharyya B, Sorkhel SK Experimental studies on Electrochemical Discharge Machining (ECDM) characteristics for machining engineering ceramics. 18th AIMTDR Conf. IIT, Kharagpur, Dec. 21-231998:322–327.
[36] Pramanik A. Developments in the non-traditional machining of particle reinforced metal matrix composites. Int J Mach Tools Manuf. 2014;86:44–61.
[37] Manna A, Malik A. Micro-drilling of Al/Al2O3-MMC on developed ECMM. Proceedings of the world congress on engineering; IAENG; 2016. (Vol. 2).
[38] Madhavi JB, Hiremath SS. Investigation on machining of holes and channels on borosilicate and sodalime glass using μ-ECDM setup. Procedia Technol. 2016;25:1257–1264.
[39] Singh T, Dvivedi A. On performance evaluation of textured tools during micro-channeling with ECDM. J Manuf Processes. 2018;32:699–713.

[40] Paul L, Hiremath SS, Babu J, et al. Effect of sensing mechanism on machining performance of ECDM process. Adv Mater Process Technol. 2021;1–10. DOI:10.1080/2374068X.2021.1945285
[41] Rajput V, Goud M, Suri NM. Performance analysis of closed-loop electrochemical discharge machining (CLECDM) during micro-drilling and response surface methodology based multi-response parametric optimisation. Adv Mater Process Technol. 2021;1–31. DOI:10.1080/2374068X.2020.1860494
[42] Torabi A, Razfar MR. The capability of ECDM in creating effective microchannel on the PDMS. Precis Eng. 2021;68:10–19.
[43] Mohan P, Manna A. Fabrication and processing of bioabsorbable hybrid Zn/(Ag + Fe + Mg)-MMC on developed ultrasonic vibration-assisted argon atmosphere stir casting set-up. Arab J Sci Eng. 2021;47(7):8361–8372.
[44] Chechi P, Maurya SK, Prasad R, et al. Microstructural and mechanical characterization of stir cast Al-SiC/flyash/graphite hybrid metal matrix composite. Mater Today Proc. 2022;64 (1):637–642.
[45] Singh L, Singh B, Saxena KK. Manufacturing techniques for metal matrix composites (MMC): an overview. Adv Mater Process Technol. 2020;6(2):441–457.
[46] Machno M. Impact of process parameters on the quality of deep holes drilled in Inconel 718 using EDD. Materials. 2019;12(14):2298.
[47] Manna A, Kundal A. An experimental investigation on traveling wire electrochemical discharge machining of hylam based composites by taguchi method. Int J Res Eng Tech Int J Adv Manuf Technol. 2013;76(1–4):29–37.
[48] Wuthrich R, Abou Ziki JD Micromachining using electrochemical discharge phenomenon: fundamentals and application of spark assisted chemical engraving. William Andrew; 2014 Nov 8.
[49] Jawalkar CS, Sharma AK, Kumar P, et al. Micromachining with ECDM: research potentials and experimental investigations. Channels. 2012;40(46):15.
[50] Rajendra KK, Sundaram M. A study on the effect of electrolyte concentration on surface integrity in micro electrochemical discharge machining. Procedia CIRP. 2016;45:355–358.
[51] Lee ES, Howard D, Liang E, et al. Removable tubing interconnects for glass-based micro-fluidic systems made using ECDM. J Micromech Microeng. 2004;14(4):535.
[52] Jain VK, Priyadarshini D. Fabrication of microchannels in ceramics (Quartz) using electrochemical spark micromachining (ECSMM). J Adv Manuf Syst. 2014;13(1):5–16.
[53] Pawariya K, Dvivedi A, Singh T. On performance enhancement of electrochemical discharge trepanning (ECDT) process by sonication of tool electrode. Precis Eng. 2019;56:8–19.
[54] Basak I, Ghosh A. Mechanism of material removal in electrochemical discharge machining: a theoretical model and experimental verification. J Mater Process Technol. 1997;71 (3):350–359.
[55] Wüthrich R, Fascio V. Machining of non-conducting materials using electrochemical discharge phenomenon—an overview. Int J Mach Tools Manuf. 2005;45(9):1095–1108.